



POLITECNICO
MILANO 1863

SCUOLA DI INGEGNERIA INDUSTRIALE
E DELL'INFORMAZIONE

MicroSat Attitude Determination And Control Performance Study

MASTER'S DEGREE IN
SPACE ENGINEERING

Authors:

Filippo Bertaboni (10706930), Politecnico di Milano
Marcello Mutti (10698636), Politecnico di Milano
Armand Petit Jacquin (10911239), ISAE ENSMA
Quentin Staller (10911457), ISAE ENSMA

Advisor: Prof. Franco Bernelli Zazzera
Group n. 7
Academic Year: 2022-23

Contents

Contents	i
1 Introduction	1
1.1 SpaceCraft Specifications	1
1.2 Mission Description	2
2 Dynamics And Kinematics	3
3 Environment	4
4 Attitude Determination	5
5 Attitude Control	7
5.1 De-tumbling	7
5.2 Slew	8
5.3 Pointing	10
5.3.1 State Observer	10
5.3.2 Gain Control	11
5.3.3 Camera	12
5.3.4 Controlled Pointing	13
5.3.5 Uncontrolled Motion	15
6 Actuators	16
7 Conclusions	18
7.1 Alternative Control	19

1 | Introduction

1.1. SpaceCraft Specifications

The subject of this study is the ESA's PROBA micro satellite. The satellite shape is that of a rectangular prism with mass of $m_{SC} = 94\text{kg}$. We define d_i as the prism dimension along the i-axis. Given the S/C relatively small dimensions, we assume the center of mass to be coincident with the geometric center. Therefore, the following inertial properties:

Axis	Dimension [m]	Moment of Inertia [$\text{kg} \cdot \text{m}^2$]	Inertial Coefficient [-]
x	$d_x = 0.8$	$I_x = 6.6583$	$K_y = 0.1529$
y	$d_y = 0.7$	$I_y = 7.8333$	$K_r = 0.2800$
z	$d_z = 0.6$	$I_z = 8.8517$	$K_p = 0.1327$

Table 1.1: S/C inertial properties. Note that the inertial coefficients are expressed in local-frame notation (yaw, roll, pitch)

Given the aforementioned hypothesis and the simple shape of the spacecraft, we consider x, y and z to be the principal inertial axes. Therefore the inertia matrix J is diagonal $J = \text{diag}\left(\begin{bmatrix} I_x & I_y & I_z \end{bmatrix}\right)$.

The satellite is equipped with three couples of star sensors and sun presence sensors. Each couple is positioned on a different face of the structure, more precisely the one identified by positive axis direction. The stars sensor has a field of view $FOV = 21.7^\circ$, and nominal angle measurement precision of $\bar{\epsilon} = 50\text{arcsec}$. The sun presence sensors have a field of view similar to that of the star sensors, scaled by a security parameter of 1.5.

For attitude control purposes an array of six thrusters is mounted on the negative z-axis face. Thrusters are labelled from F_1 to F_6 . In the following table their position and exhaust direction:

$r_1 = \begin{bmatrix} \frac{d_x}{2} \\ -\frac{d_y}{2} \\ -\frac{d_z}{2} \end{bmatrix}$	$r_2 = \begin{bmatrix} \frac{d_x}{2} \\ \frac{d_y}{2} \\ -\frac{d_z}{2} \end{bmatrix}$	$r_3 = \begin{bmatrix} 0 \\ \frac{d_y}{2} \\ -\frac{d_z}{2} \end{bmatrix}$	$r_4 = \begin{bmatrix} -\frac{d_x}{2} \\ \frac{d_y}{2} \\ -\frac{d_z}{2} \end{bmatrix}$	$r_5 = \begin{bmatrix} -\frac{d_x}{2} \\ -\frac{d_y}{2} \\ -\frac{d_z}{2} \end{bmatrix}$	$r_6 = \begin{bmatrix} 0 \\ -\frac{d_y}{2} \\ -\frac{d_z}{2} \end{bmatrix}$
$\hat{F}_1 = \hat{x}$	$\hat{F}_2 = \hat{x}$	$\hat{F}_3 = \hat{y}$	$\hat{F}_4 = -\hat{x}$	$\hat{F}_5 = -\hat{x}$	$\hat{F}_6 = -\hat{y}$

Table 1.2: Thrusters position and exhaust direction

It is possible to compute the thruster configuration matrix:

$$\left[\hat{R} \right] = \begin{bmatrix} 0 & 0 & \frac{d_z}{2} & 0 & 0 & -\frac{d_z}{2} \\ -\frac{d_z}{2} & -\frac{d_z}{2} & 0 & \frac{d_z}{2} & \frac{d_z}{2} & 0 \\ \frac{d_y}{2} & -\frac{d_y}{2} & 0 & \frac{d_y}{2} & -\frac{d_y}{2} & 0 \end{bmatrix} \quad (1.1)$$

The thrusters operate using pulsed plasma, with actuation force $\bar{F} = 10^{-3} N$.

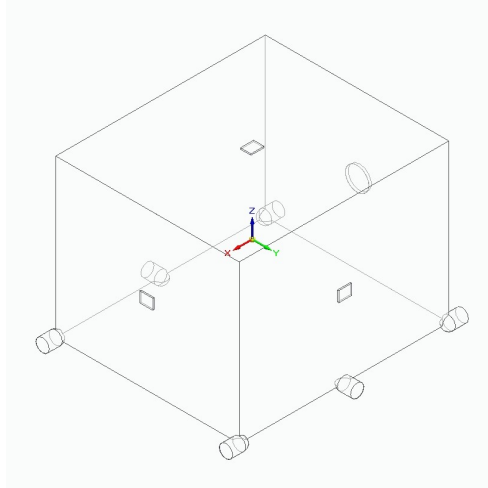


Figure 1.1: 3D model representation of the satellite

1.2. Mission Description

PROBA operates on a circular sun synchronous orbit. For the purpose of the study, since the execution time of each simulation is equal or less to the orbital period T_o , orbital parameters J2 variation can be neglected.

Below the set of keplerian elements:

Height	$H[km]$	515
Eccentricity	$e[-]$	0
Inclination	$i[deg]$	97.5
RAAN	$\Omega[deg]$	0
Anomaly of Periapsis	$\omega[deg]$	0

Table 1.3: Orbital parameters. Note that the orbit is retrograde.

The period of the orbit T_o is computed as $T_o = 2\pi\sqrt{\frac{R^3}{\mu}}$, where μ is Earth gravitational constant, and $R = R_E + H$ is the radius of the orbit. The purpose of the mission is Earth monitoring. Control is acted upon the spacecraft to keep it aligned to the LVLH frame.

The spacecraft is equipped with a camera located on the negative x-axis face for the purpose of Earth monitoring. It's pointing system requires precision of $nad = 2^\circ$.

2 | Dynamics And Kinematics

The dynamic of the spacecraft is described using Euler's Equations. Given \mathbf{T} the overall external torque, sum of control and disturbances, given J the spacecraft inertia matrix, it's possible to compute the satellite's angular velocity $\boldsymbol{\omega}$ expressed in body-frame components. The attitude of the spacecraft is determined through propagation of Euler Angles, which are then used to compute the direction cosine matrix A .

In particular, it was decided to use the 312 and 313 sequences, having implemented a switching algorithm to avoid singularity.

The 312 sequence is singular if $\theta = \frac{\pi}{2} + n\pi$, given $\theta = \arccos(A_{33})$.

The 313 sequence is singular if $\theta = n\pi$, given $\theta = \arccos(A_{23})$.

Given the initial direction cosine matrix A_0 , at time t_0 , the system determines which method to initially use. The Euler Angles are then propagated in time, maintaining the initial propagation sequence unless θ is in the range of 10° of the singularity value. In case of this happening, the direction cosine matrix is computed using the current sequence, only for it to be decomposed in the other sequence, which is then used until a switch is again required.

Regardless of the sequence in use, both the Euler Angles integration systems compute the direction cosine matrix $A_{b/n}$, which indicates the attitude of the spacecraft body-frame with respect to the Earth-centered equatorial inertial frame.

3 | Environment

Given the spacecraft orbit parameters 1.3, given θ_0 the initial true anomaly, it is possible to compute its position \mathbf{r}_n^{SC} with respect to the inertial frame. Along with the position, the attitude of the local frame $A_{l/n}$ is computed. The local frame is so that $\hat{\mathbf{x}}_{l/n} = \hat{\mathbf{r}}_n^{SC}$ and $\hat{\mathbf{y}}_{l/n} = \hat{\mathbf{v}}_n^{SC}$. During its motion along the orbit, the spacecraft is subjected to four main environmental effects, in the form of disturbance torques. These disturbances are due to the spacecraft gravity gradient (GG), the interaction of its electrical magnetic dipole with Earth's magnetic field (M), solar radiation pressure (SRP), and atmospheric air drag (AD). Using the following equations, it is possible to estimate the order of magnitude of the maximum torque each disturbance can act upon S/C:

$$\left\{ \begin{array}{l} T_M^{GG} = \frac{3\mu_e}{2r_n^{SC^3}} (I_M - I_m) \\ T_M^M = D_s B_M \\ T_M^{SRP} = P_s A_s (1 + q) (c_{sp} - c_g) \\ T_M^{AD} = \frac{1}{2} \rho v^2 A_s c_D (c_{ap} - c_g) \end{array} \right. \quad \begin{array}{l} (3.1a) \\ (3.1b) \\ (3.1c) \\ (3.1d) \end{array}$$

The spacecraft internal magnetic dipole is set to $\mathbf{m}^1 = [0.37 \ 0.32 \ 0.28] \text{ Am}^2$.

While the effects of gravity gradient and magnetic disturbance are comparable in magnitude, the effects of solar radiation pressure and air drag can be assumed to be negligible, as they are estimated to be two or more orders of magnitude smaller. Given the low orbital height and the orbital plane high inclination, it was decided to model the magnetic field up to order five, to more accurately describe the polar anomalies.

¹The magnitude of \mathbf{m} was chosen in accordance with data presented in Table IV from NASA SP-8018 "Spacecraft Magnetic Torques", March 1969

4 | Attitude Determination

As introduced in section 1.1, the spacecraft is equipped with three star sensors. The sensors operate with sampling frequency of $f_S = 1Hz$, therefore the attitude determination systems, and consequently the control system, operate with discrete signals of sample time $T_s = 1s$. The sensors are positioned on orthogonal surfaces, in order to maximise the *orthogonality* of the measurements.

Each of the sensor determines when one or more stars is in its field of view and evaluates the star's position in the body frame. The same star is selected from the catalogue, where its inertial position is stored.

Sun presence sensors are coupled to each star sensor, in order to turn them off individually in case the sun is in the field of view. This way, the attitude determination system at every time instant always gets at least two readings, at most three.

Every measurement is expressed as $\mathbf{s}_{b,i}$, orientation of the i-th star in the catalogue, in the form of two angles ϕ, λ so that:

$$\mathbf{s}_{b,i} = \begin{bmatrix} -\sin(\phi + \Delta\phi) \cos(\lambda + \Delta\lambda) \\ \cos(\phi + \Delta\phi) \cos(\lambda + \Delta\lambda) \\ \sin(\lambda + \Delta\lambda) \end{bmatrix} \approx \mathbf{s}_{s,i} = \begin{bmatrix} -\sin(\phi) \cos(\lambda) \\ \cos(\phi) \cos(\lambda) \\ \sin(\lambda) \end{bmatrix} = A_{s/b_k} A_{b/n} \mathbf{s}_{n,i} \quad (4.1)$$

$\Delta\phi$ and $\Delta\lambda$ represent reading error. The values are randomly picked from a normal distribution of variance σ^2 and mean $\mu = 0$. σ is given as $\sigma = \epsilon$, where ϵ is the error associated to the angle measurement of the sensors. It has a minimum nominal value of $\bar{\epsilon} = 50arcsec$, but it is modelled to be proportional to angular velocity so that:

$$\epsilon_i = \bar{\epsilon} + \omega_i \quad (4.2)$$

The index $i = 1 : 3$ represents the sensor pointing direction and the associated angular velocity. Every reading is also disturbed by bias error. That is due to each sensor's mounting error, expressed as:

$$A_{s/b_k} = R_j(\alpha) R_k(\beta) R_j(-\alpha) \quad (4.3)$$

The index k refers to the sensor, more precisely to the k-axis direction of the face it is mounted on. j is one of the remaining axis, so that $j \neq k$.

The angles α and β are taken randomly from the intervals $[0, 2\pi]$ and $[0, x]$ respectively, using $x = 0.001^\circ$.

The measured attitude is obtained by solving the Wabha's Problem: the solution is expressed in the form of the direction cosine matrix $A_{b/n}^*$.

Given the measured attitude $A_{b/n}^*$, it is also possible to evaluate the angular velocity as:

$$[\boldsymbol{\omega}^* \wedge] = \begin{bmatrix} 0 & -\omega_z^* & \omega_y^* \\ \omega_z^* & 0 & -\omega_x^* \\ -\omega_y^* & \omega_x^* & 0 \end{bmatrix} = -\frac{d}{dt} \left(A_{b/n}^* \right) A_{b/n}^{*T} \quad (4.4)$$

The measured angular velocity $\boldsymbol{\omega}^*$ is computed by taking the mean value of the extra-diagonal components:

$$\omega_x^* = \frac{[\boldsymbol{\omega}^* \wedge]_{3,2} - [\boldsymbol{\omega}^* \wedge]_{2,3}}{2} \quad (4.5a)$$

$$\omega_y^* = \frac{[\boldsymbol{\omega}^* \wedge]_{1,3} - [\boldsymbol{\omega}^* \wedge]_{3,1}}{2} \quad (4.5b)$$

$$\omega_z^* = \frac{[\boldsymbol{\omega}^* \wedge]_{2,1} - [\boldsymbol{\omega}^* \wedge]_{1,2}}{2} \quad (4.5c)$$

Note that instead of simply being extracted from $[\boldsymbol{\omega}^* \wedge]$, the velocity components are extracted and averaged. Due to the perturbation introduced to the measurements, $A_{b/n}^*$ is not perfectly orthonormal. Therefore $[\boldsymbol{\omega}^* \wedge]$ is not perfectly anti-symmetric, hence 4.5.

5 | Attitude Control

The attitude control system is responsible for elaborating the ideal control torque \mathbf{T}_c , given the determined attitude and velocity.

It's possible to divide the mission into three distinct phases, each characterized by different requirements and therefore different control strategies:

- De-tumbling: as the satellite is released from the launches, it's injected into orbit with uncontrolled angular velocity $\boldsymbol{\omega}$. The first objective is to slow down the rotation by bringing $|\boldsymbol{\omega}| \approx 0 \text{ rad/s}$.
- Slew: the satellite is oriented so that its attitude approximates the configuration required by mission constraints.
- Pointing: the satellite is controlled and maneuvered in the proximity of the configuration required by mission constraints.

The objective of the mission is Earth monitoring, so the spacecraft has to perform nadir pointing. Therefore the aforementioned configuration is $A_{b/n} \approx A_{l/n}$.

5.1. De-tumbling

During the de-tumbling phase the control parameters are ω_x , ω_y and ω_z . Therefore both attitude and angular velocity determination systems are required.

At insertion, initial attitude and velocity are unknown and unpredictable, therefore the control system has to operate non-linear control. Three PD controllers operate separately on the three angular velocity components. Following, the equation of PD control:

$$PD(z) = K_P + K_D \frac{z - 1}{T_s z} \quad (5.1)$$

The coefficients K_P , K_D are respectively the proportional coefficient and the derivative coefficients respectively. All three controllers share the same parameters, chosen via trial and error tests using the Ziegler-Nichols method as $K_P = 0.035$ and $K_D = 0.004$.

The initial angular velocity components are chosen as random values in the order of 10^{-2} .

In $\Delta t_{det} = 40\text{min}50\text{s}$ the angular velocity is reduced by a factor of approximately 300, down to order of magnitude 10^{-4} .

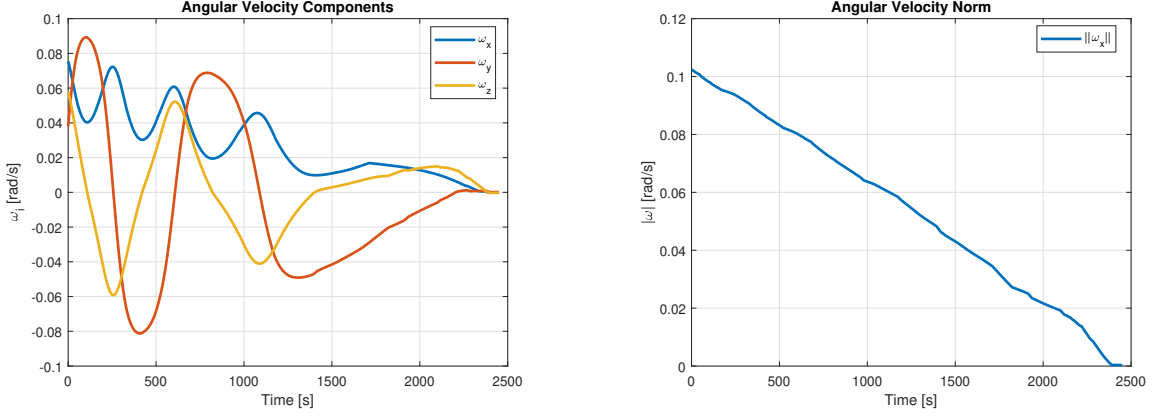


Figure 5.1: Angular velocity components and norm during de-tumbling phase

The control torque required to further reduce tumble does not exceed the thrusters activation threshold, therefore the next mission phase begins.

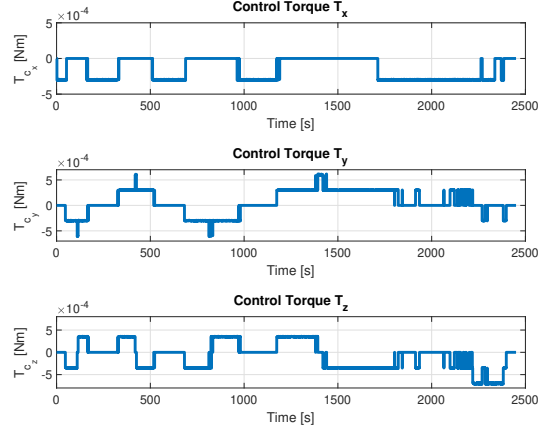


Figure 5.2: Individual axis control torque during de-tumbling phase

5.2. Slew

Once the spacecraft has been de-spun, the satellite has to align body-frame $A_{b/n}$ to the orbit local frame $A_{l/n}$. Given the true anomaly $\theta(t)$ of S/C at time t , it is possible to compute $A_{l/n}$ as:

$$A_{l/n} = R_3(\theta(t) + \omega) R_1(i) R_3(\Omega) \quad (5.2)$$

It is possible to compute the attitude error in the form of:

$$A_e = A_{b/l} = A_{b/n} A_{l/n}^T \quad (5.3)$$

Assuming $A_{b/n} \approx A_{l/n}$, then $A_e \approx I$, in particular:

$$A_e \approx \begin{bmatrix} 1 & \alpha_z & -\alpha_y \\ -\alpha_z & 1 & \alpha_x \\ \alpha_y & -\alpha_x & 1 \end{bmatrix} \quad (5.4)$$

α_x , α_y and α_z are small angle error, and they can be computed in a similar fashion to equation 4.5:

$$\alpha_x = \frac{(A_e)_{2,3} - (A_e)_{3,2}}{2} \quad (5.5a)$$

$$\alpha_y = \frac{(A_e)_{3,1} - (A_e)_{1,3}}{2} \quad (5.5b)$$

$$\alpha_z = \frac{(A_e)_{1,2} - (A_e)_{2,1}}{2} \quad (5.5c)$$

Since the task of the de-tumbling maneuver is to simply reduce the angular velocity of the spacecraft, the attitude $A_{b/n}$ and the end of the maneuver is not controlled. Therefore, we must assume that pointing control is again operating outside linearity, far from the desired equilibrium state. Such state would be $A_{b/n} = A_{l/n}$, or $\alpha_x = \alpha_y = \alpha_z = 0$.

Despite the non-linearity of the problem, it's still possible to correct the attitude by using PD controllers (5.1) on the α_i parameters. After initial transitory phase, $\alpha_i, i = 1 : 3$ are brought to the vicinity of 0 rad.

PD coefficients are set to $K_P = 6 \cdot 10^{-4}$ and $K_D = 5.625 \cdot 10^{-2}$.

After the maneuver, $\alpha_i, i = 1 : 3$ are small enough to apply small angles hypothesis and therefore assume linearity.

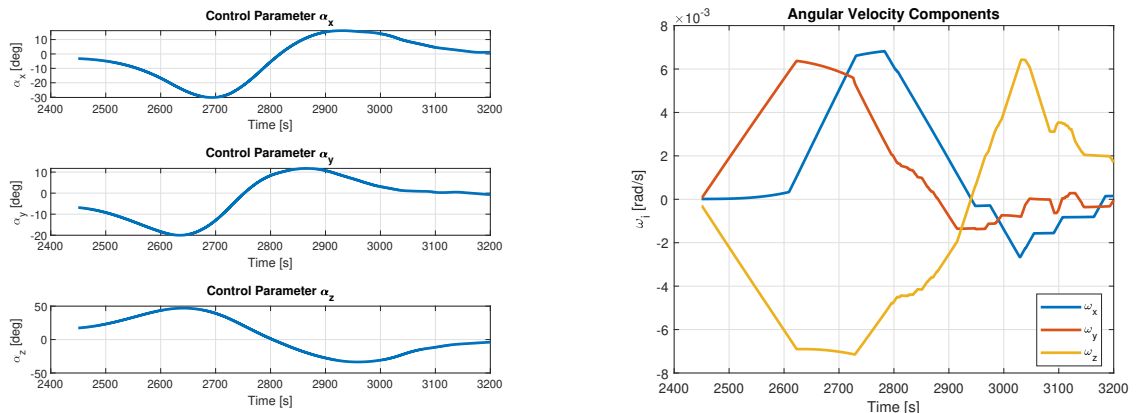


Figure 5.3: Control parameters α_i and angular velocity components during slew phase

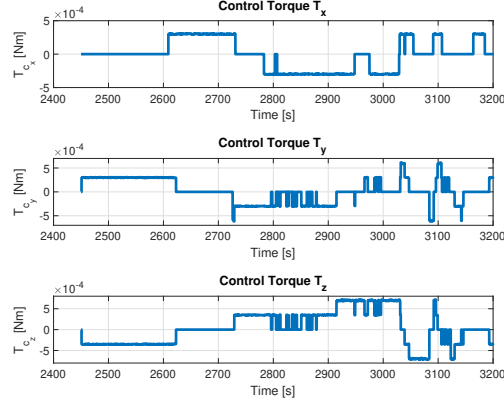


Figure 5.4: Individual axis control torque during slew phase

5.3. Pointing

After slew phase α_i , computed in the same fashion as 5.5, are such that $|\alpha_i| \leq 5^\circ, i = 1 : 3$. It is therefore possible to switch control method to take advantage of the problem linearity. Such control method combines the use of state observer and proportional control.

5.3.1. State Observer

The state observer is a dynamic system capable of yielding an estimation of the state of the spacecraft, given that S/C is operating around a specified equilibrium point.

Dynamics, kinematics and attitude determination can be described as a state space system of input \mathbf{u} the total torque acting on the satellite, and output \mathbf{y} the difference between the measured control parameters $\alpha_x, \alpha_y, \alpha_z$, and their desired value $\alpha_{x_d}, \alpha_{y_d}, \alpha_{z_d}$.

We temporarily assume $\alpha_{x_d} = \alpha_{y_d} = \alpha_{z_d} = 0$, S/C is idle.

The hypothesis of linearity allows to compute $\boldsymbol{\omega}$ as:

$$\begin{bmatrix} \omega_x \\ \omega_y \\ \omega_z \end{bmatrix} = \begin{bmatrix} \dot{\alpha}_x \\ \dot{\alpha}_y \\ \dot{\alpha}_z \end{bmatrix} + A_{l/n} \begin{bmatrix} 0 \\ 0 \\ n \end{bmatrix} \quad (5.6)$$

n is the mean angular velocity of the satellite along the orbit, and is computed as $n = \frac{2\pi}{T_o}$. Combining Euler's Equations with 5.6 it is possible to describe the motion of the satellite with respect to the LVLH local frame. Linearizing the so found equations around $\dot{\alpha}_i = \alpha_i = T_i = 0, i = 1 : 3$, it is possible to determine the matrices of the aforementioned state space:

$$A = \begin{bmatrix} 0 & (1 - K_y)n & 0 & -K_y n^2 & 0 & 0 \\ (K_r - 1)n & 0 & 0 & 0 & -4K_r n^2 & 0 \\ 0 & 0 & 0 & 0 & 0 & -3K_p n^2 \\ 1 & 0 & 0 & 0 & 0 & 0 \\ 0 & 1 & 0 & 0 & 0 & 0 \\ 0 & 0 & 1 & 0 & 0 & 0 \end{bmatrix} \quad (5.7)$$

$$B = \begin{bmatrix} \frac{1}{I_x} & 0 & 0 \\ 0 & \frac{1}{I_y} & 0 \\ 0 & 0 & \frac{1}{I_z} \\ 0 & 0 & 0 \\ 0 & 0 & 0 \\ 0 & 0 & 0 \end{bmatrix}, C = \begin{bmatrix} 0 & 0 & 0 & 1 & 0 & 0 \\ 0 & 0 & 0 & 0 & 1 & 0 \\ 0 & 0 & 0 & 0 & 0 & 1 \end{bmatrix}, D = \begin{bmatrix} 0 & 0 & 0 \\ 0 & 0 & 0 \\ 0 & 0 & 0 \end{bmatrix}$$

Below the state \mathbf{x} , input \mathbf{u} and output \mathbf{y} :

$$\mathbf{x} = [\dot{\alpha}_x \quad \dot{\alpha}_y \quad \dot{\alpha}_z \quad \alpha_x \quad \alpha_y \quad \alpha_z]^T, \mathbf{u} = [T_x \quad T_y \quad T_z]^T, \mathbf{y} = [\alpha_x \quad \alpha_y \quad \alpha_z]^T \quad (5.8)$$

The observer's matrix L is computed through pole placement, so that $\hat{A} = A - LC$ has eigenvalues $\lambda = -[0.04 \quad 0.04 \quad 0.04 \quad 0.05 \quad 0.05 + 0.025i \quad 0.05 - 0.025i]^T$.

Such poles are chosen to guarantee convergence of the observed state $\hat{\mathbf{x}}$ to the system state \mathbf{x} , without many oscillations. It ought to be noted that such eigenvalues could have much smaller $Re(\lambda_i)$ for faster convergence. It was however observed that lowering $Re(\lambda_i)$ does yield noticeable improvement.

5.3.2. Gain Control

Assuming that after brief initial transitory $\hat{\mathbf{x}} \approx \mathbf{x}$, control torque \mathbf{u} can be computed as $\mathbf{u} = K\hat{\mathbf{x}}$. K is the solution of the linear-quadratic regulator design with output weighting. It is function of the linearized system 5.7, and the weighting matrices Q_c , R_c defined as:

$$Q_c = diag \left\{ \left[1/\alpha_{x_{lim}}^2 \quad 1/\alpha_{y_{lim}}^2 \quad 1/\alpha_{z_{lim}}^2 \right] \right\} \quad (5.9a)$$

$$R_c = diag \left\{ \left[1/T_{lim}^2 \quad 1/T_{lim}^2 \quad 1/T_{lim}^2 \right] \right\} \quad (5.9b)$$

Proportional control acts to keep the control parameters within the specified limits.

The constraints α_y, α_z are determined by mission requirements on pointing accuracy nad . Given that $nad = 2^\circ$, then $\alpha_{y_{lim}} = \alpha_{z_{lim}} = 1.9nad$. Mission requirements do not constrain α_x , but $\dot{\alpha}_x$, as ω_x needs to be limited in order for the camera to provide precise imaging. However, direct control on α_x is required to keep the control system in the range of linear operability. It can be proved that $\dot{\alpha}_i$ are at all times in an acceptable range, and therefore don't need direct control.

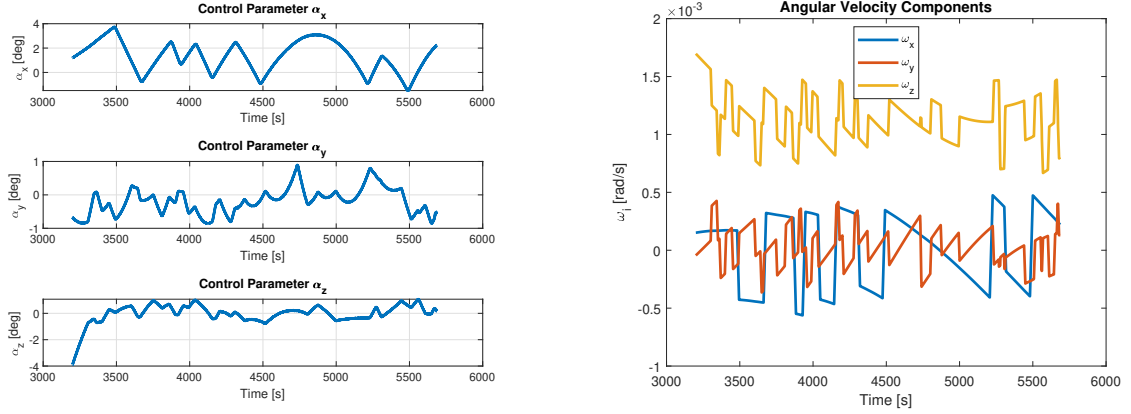


Figure 5.5: Control parameters α_i and angular velocity components during idle pointing phase

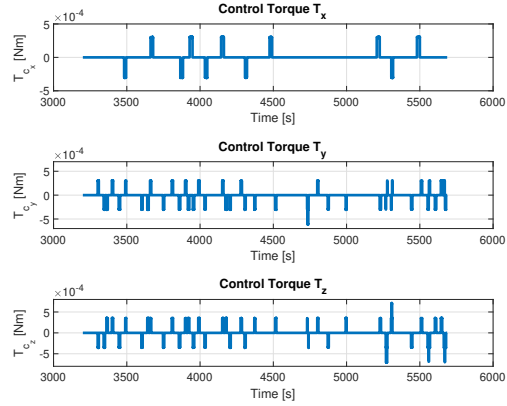


Figure 5.6: Individual axis control torque during idle pointing phase

5.3.3. Camera

The camera is the main apparatus for Earth imaging. As mentioned in 1.1 the mission requires a pointing precision of $nad = 2^\circ$. Given the orbit height H such requirement roughly translates into a square of $18km \cdot 18km$.

To visualize the angular displacement of the camera axis two angles λ and ϕ are defined to represent the vertical and horizontal displacement with respect to the nadir direction and the orbital plane. Given the attitude error $A_e = A_{b/l}$, $x_{b/l}$ is the spacecraft x-axis represented in LVLH coordinates:

$$\mathbf{x}_{b/l} = (A_{b/l})_{1,:} = \begin{bmatrix} \cos(\lambda) \cos(\phi) \\ \cos(\lambda) \sin(\phi) \\ \sin(\lambda) \end{bmatrix} \quad (5.10)$$

Therefore:

$$\begin{aligned}\phi &= \tan^{-1} \left(\frac{(\mathbf{x}_{b/l})_2}{(\mathbf{x}_{b/l})_1} \right) \\ \lambda &= \sin^{-1} \left((\mathbf{x}_{b/l})_3 \right)\end{aligned}\quad (5.11)$$

Since the control system is operating in the proximity of the equilibrium configuration it is possible to verify that $\lambda \approx -\alpha_y$ and $\phi \approx \alpha_z$.

Note that despite same nomenclature as 4.1, λ and ϕ are proper of the pointing system.

Below, the computed pointing precision in the last orbital phase:

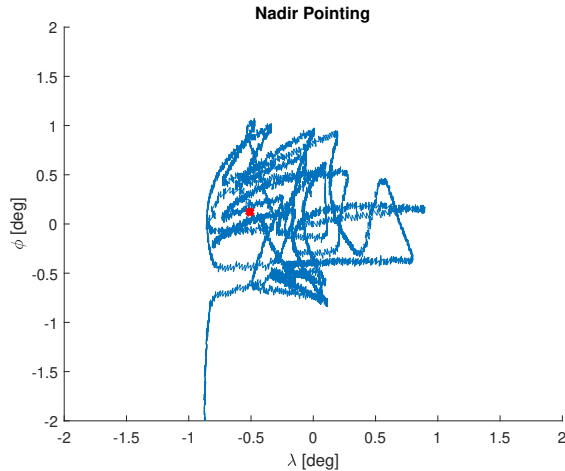


Figure 5.7: Pointing accuracy during idle pointing phase. \circ represents initial state, while \times represents final state

5.3.4. Controlled Pointing

In the previous sections, the performance of the control system was evaluated with respect to the objective of keeping the spacecraft frame aligned with the local orbital frame. In other words the desired attitude was set to $\alpha_{x_d} = \alpha_{y_d} = \alpha_{z_d} = 0$.

As the state observer operates to minimize inputs $e_i = \alpha_i - \alpha_{i_d} \rightarrow 0$, by setting $\alpha_{i_d} \neq 0$ and granted that the system does not diverge from linearity, the control parameters α_i will approximate the desired state α_{i_d} .

To demonstrate the spacecraft maneuvering capabilities it is possible to prescribe α_{i_d} as functions of time. Below a demonstrative example:

$$\begin{cases} \alpha_{y_d} = a_y \sin(2\pi f_y t) \\ \alpha_{z_d} = a_z \sin(2\pi f_z t) \end{cases}, \begin{cases} a_y = 5^\circ, f_y = \frac{8}{T_o} \\ a_z = 15^\circ, f_z = \frac{4}{T_o} \end{cases} \quad (5.12)$$

Oscillations of α_y entail oscillations of the camera scope between the hemispheres defined by the orbital plane. Oscillations of α_z instead entail that the scope anticipates or trails spacecraft

position.

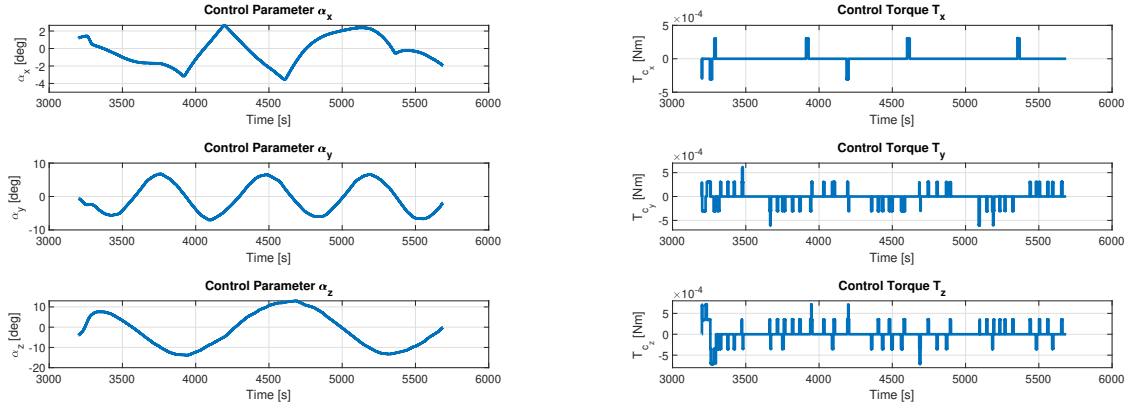


Figure 5.8: Control parameters α_i and individual axis control torque

Note that, as seen from figure 5.9, the control parameters are subjected to the same precision requirements set in equation 5.9. Therefore $\alpha_i \approx \alpha_{id} \pm \alpha_{ilim}$.

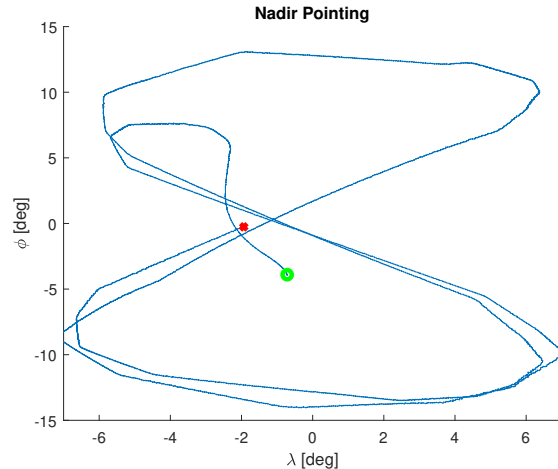


Figure 5.9: Pointing accuracy during controlled pointing phase. \circ represents initial state, while \times represents final state

5.3.5. Uncontrolled Motion

It is possible to observe the motion of the spacecraft assuming no control torque is applied. Due to the spacecraft inertial properties, it can be proved that its major inertia axis I_z is stable with respect to the gravity gradient disturbance torque. This property however does not contribute to the mission required stability. Therefore control is required to prevent the spacecraft to diverge from its pointing attitude.

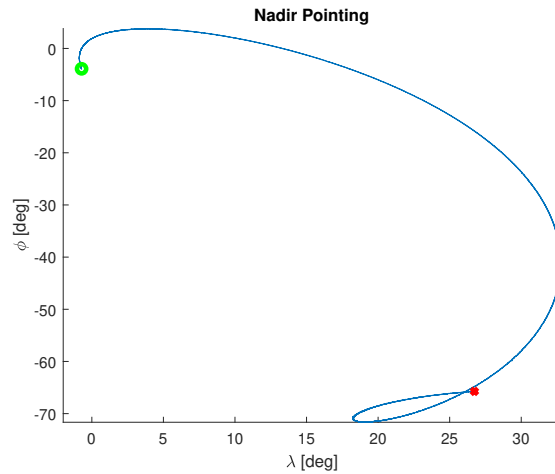
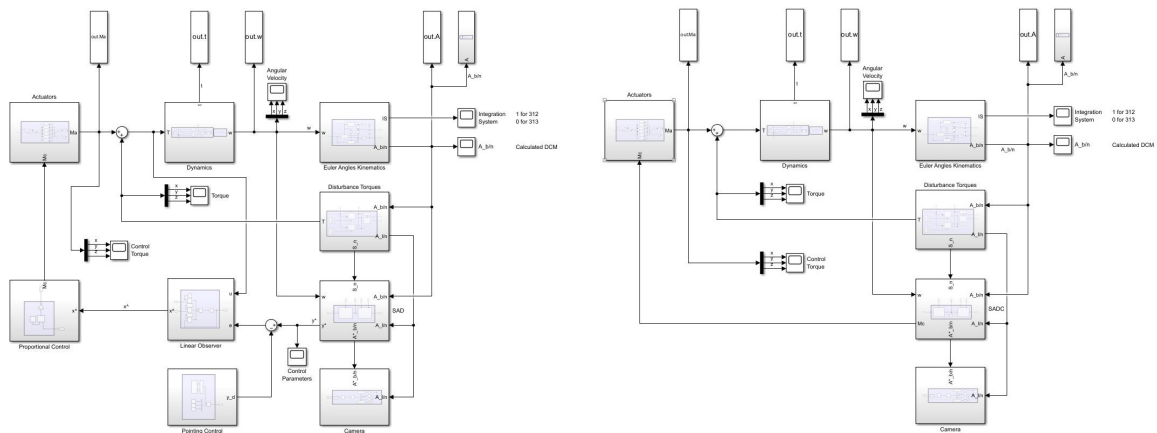


Figure 5.10: Pointing accuracy without attitude control system. \circ represents initial state, while \times represents final state

Control Schematics



Side by side the ADCS schematics for poiting (left) and slew (right) control. The ADCS schematics for de-tumbling control is similar to pointing, with the addition of angular velocity determination. De-tumbling ADCS also lacks the camera component, as it is not active before S/C is de-spun.

6 | Actuators

Regardless of the mission phase, the active control system receives as input a set of control parameters and outputs the control torque $\mathbf{T}_c = [T_{x_c} \ T_{y_c} \ T_{z_c}]^T$, whose components have arbitrary magnitude and sign.

As aforementioned in chapter 1.1, the spacecraft control actuation system is composed of six thrusters of configuration $[\hat{R}]$ ^{1.1}. Each thruster actuation is binary, meaning that it can only either be deactivated or activated with fixed constant thrust \bar{F} . Given the satellite inertial properties and operational requirements it was decided to use thrusters of thrust $\bar{F} = 10^{-3}$, which is typical of electric pulsed plasma thrusters (PPTs).

As the name suggests, PPTs generate thrust by pulses of accelerating plasma. It ought to be noted that such bursts are anticipated and followed by inactive time, due to electrical charge and discharge of the system. However, even accounting for such downtime the overall PPTs burst frequency is typically in the order of microseconds. Given the time scale of the simulation, and its temporal discretization, we assume the thrust to be constant disregarding charge and discharge time¹

Given the thrusters configuration matrix $[\hat{R}]$, its pseudo-inverse $[\hat{R}]^*$ and $\mathbf{w} = [1 \ 1 \ 1 \ 1 \ 1 \ 1]^T$ the null space vector of $[\hat{R}]$, it is possible to compute the control thrust so that each value F_{i_c} is non-negative:

$$[F_{1_c} \ F_{2_c} \ F_{3_c} \ F_{4_c} \ F_{5_c} \ F_{6_c}]^T = [\hat{R}]^* \mathbf{T}_c + \mathbf{w} \cdot \max_{i=1:6} ([\hat{R}]^* \mathbf{T}_c) \quad (6.1)$$

Given the binary behaviour of each thruster, a logic activation switch is required to individually interface with each of them.

One upper and lower thresholds are defined, respectively upper activation threshold $UL = 10^{-4}$ and lower deactivation threshold $LL = 10^{-5}$.

As denoted by the following hysteresis graph, the actuators will turn on once $T_{i_c} > UL$, and will keep burning until $T_{i_c} < LL$, producing a thrust of either $F_{i_a} = 0$ or $F_{i_a} = \bar{F}$.

¹PPTs data were derived from "Journal of Propulsion and Power" Vol14, No. 5, September-October 1998

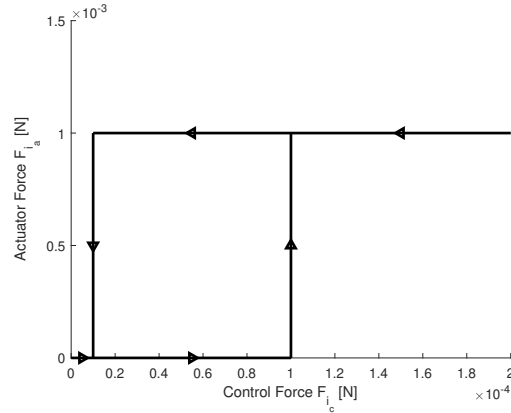


Figure 6.1: Hysteresis behavior of logic switch

Once $F_{i_a}, i = 1 : 6$ have been computed, their magnitude is perturbed to simulate thrust inconsistencies so that $F_{i_a} = \bar{F} \pm 3\%$. In order to simulate possible mounting errors, the control torque is further disturbed using $T_p = R_{123}(a_x, a_y, a_z) \approx I$. a_x, a_y, a_z were randomly selected in the range $[-0.03^\circ, 0.03^\circ]$. It is then possible to compute the effective control torque acting on the spacecraft as:

$$\mathbf{T}_c = [T_{x_c} \quad T_{y_c} \quad T_{z_c}]^T = T_p [\hat{R}] [F_{1a} \quad F_{2a} \quad F_{3a} \quad F_{4a} \quad F_{5a} \quad F_{6a}]^T \quad (6.2)$$

7 | Conclusions

Below, the different mission phases patched together:

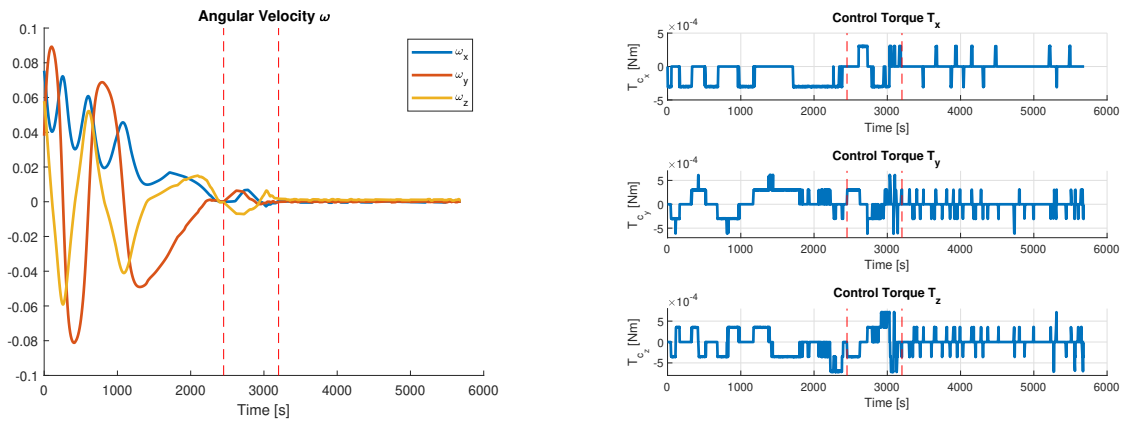


Figure 7.1: Overall angular velocity components and individual axis control torque during de-tumbling, slew and idle pointing phases

De-tumbling phase duration: Slew phase duration: Idle pointing phase duration:	$\Delta t_{det} = 40\text{min}50\text{s}$ $\Delta t_{po} = 14\text{min}10\text{s}$ $\Delta t_{sl} = T_o - (\Delta t_{det} + \Delta t_{po}) \approx 39\text{min}46.73\text{s}$
--	---

It can be observed that de-tumbling and slew are the most expensive maneuvers of the mission. Given \bar{F} , the control torque produced is limited, therefore de-tumbling is particularly lengthy and requires frequent and continuous burn. At the same time, since the thrust cannot be modulated in magnitude, and during three-axis control pointing phase the control system manifests *oscillating* behavior.

Undoubtedly, reaction wheels would have provided more precise control actuation. The aforementioned behavior of thrust control hints at the possibility of the reaction wheels to operate saturation free for long time periods. The performance of reaction-wheels-based control will be evaluated in the following section.

It is however fair to observe that the satellite is capable of operating efficiently relying only on PPTs.

7.1. Alternative Control

In order to preserve fuel and maximize pointing accuracy a different control strategy was explored: the use of two reaction wheels to actuate control along the y and z axis. It's possible to compute the torque imprinted by each wheel as:

$$\begin{bmatrix} \dot{h}_y \\ \dot{h}_z \end{bmatrix} = -A_{RW}^* \left(T_c + \omega^* \wedge A \begin{bmatrix} h_y \\ h_z \end{bmatrix} \right) \quad (7.1)$$

A_{RW} is the reaction wheel configuration matrix, A_{RW}^* its pseudoinverse.

It's possible to introduce bias mounting error in the same fashion as 6.1 using T_p . Then the actual control torque:

$$T_c = T_p \left(-\omega \wedge A_{RW} \begin{bmatrix} h_y \\ h_z \end{bmatrix} - A \begin{bmatrix} \dot{h}_y \\ \dot{h}_z \end{bmatrix} \right) \quad (7.2)$$

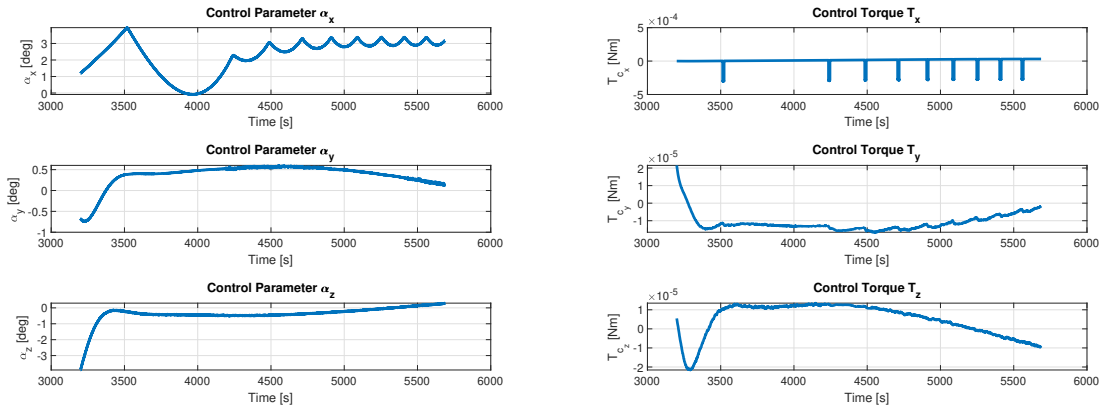


Figure 7.2: Control parameters α_i and individual axis control torque

As expected, the pointing precision of the system is greatly improved, while at the same time the maneuvering cost is considerably reduced. Reaction wheels might reach saturation, in such case thrust control might intervene to permit spin-down and resume operations.

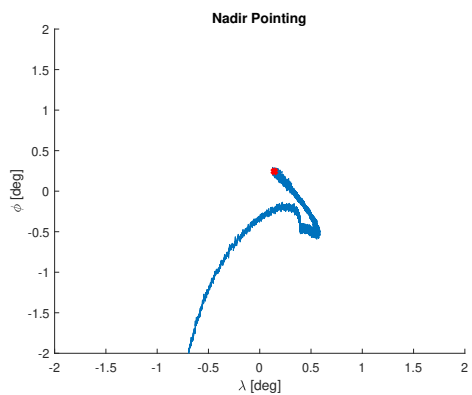


Figure 7.3: Pointing accuracy without attitude control system. \circ represents initial state, while \times represents final state